Theoretical Evaluation of Several Possible Along-Track InSAR Modes of TerraSAR-X for Ocean Current Measurements

Roland Romeiser, *Member, IEEE*, and Hartmut Runge

***Abstract*—The German satellite TerraSAR-X, scheduled for launch in late 2006, will permit high-resolution ocean current measurements by along-track interferometric SAR (along-track InSAR) in various experimental modes of operation, using different sections of its X-band SAR antenna array with a total length of 4.8 m as individual receive antennas. Depending on antenna and receive-chain settings, effective InSAR time lags of about 0.17 to 0.29 ms can be realized in combination with different noise levels, single-look resolutions, swath widths, and incidence angles. We give an overview of the characteristics of the possible InSAR modes and evaluate their suitability for current measurements on the basis of simulated data products. Our results indicate that the quality of interferometric stripmap data from TerraSAR-X will be clearly superior to the quality of the existing data acquired over the Dutch coast during the Shuttle Radar Topography Mission; accurate current retrievals can be expected at effective spatial resolutions on the order of 500 m. However, in modes using a multiplexed single receive chain, the effective swath width of stripmap data will be limited to only 15 km, while dual receive-chain operation offers a swath width of 30 km for stripmap data and promises a reasonable data quality even for ScanSAR data with a maximum swath width of 100 km. Finally, we consider fundamental relations between along-track baseline, instrument noise, and resulting InSAR phase noise to discuss the potential for current measuring performance improvements of TerraSAR-X follow-on satellites.**

***Index Terms*—Along-track interferometry (ATI), current measurements, interferometric synthetic aperture radar (InSAR), TerraSAR-X.**

I. Introduction

INTERNATIONAL user requirement surveys (e.g., [1]) have identified a strong demand for repeated high-resolution current measurements in coastal areas. Promising applications would be, for example, the generation of tidal atlases, the development, validation, and operation of numerical circulation models and corresponding data assimilation schemes, the monitoring of bathymetric changes, pollution monitoring, river runoff monitoring, the siting of tide-driven electric power plants, ship traffic advisory, and many other applications with commercial, socio-economic, and/or scientific backgrounds. Until now, current measurements have been obtained mainly as point measurements from *in situ* instruments such as mechanical current meters or acoustic Doppler current profilers. A spatial coverage of a few 1000 km^2 with a resolution in the kilometer range (and a continuous temporal coverage) can be obtained from ground-based HF radars (e.g., [2]), which are used for operational monitoring activities at many locations around the world, but require time-consuming and costly infrastructural preparations if they are to be used for individual experiments at remote locations.

An attractive new development offering a higher spatial resolution than HF radar and the flexibility to perform measurements anywhere in the world from airborne or spaceborne platforms is the along-track interferometric synthetic aperture radar (along-track InSAR), which was first proposed in [3] in 1987. In principle, the along-track interferometry (ATI) permits the imaging of line-of-sight surface velocity fields with the spatial resolution and coverage (swath width) of a SAR, which is usually on the order of meters. This is achieved by acquiring two SAR images of the same scene with a short time lag on the order of milliseconds, which exhibit phase differences proportional to Doppler shifts of the backscattered signal and, thus, to target velocity components in the radar look direction. The feasibility of current measurements by ATI has been demonstrated in a number of experiments with airborne prototype instruments (e.g., [4]–[6]). Technically, some of the existing airborne systems would be available for routine measurements, but due to their experimental character and due to the costs and logistical requirements of airborne imaging radar operations, the market for operational airborne ATI services has been very limited until now.

This may change with the implementation of spaceborne along-track InSAR systems, which just need to be switched on during overpasses of any test area of interest to obtain repeated and consistent current-field observations without major efforts and at reasonable effective costs. Theoretical concepts of spaceborne InSAR configurations have already been discussed in several publications and project reports (e.g., [7]–[9]). A first demonstration of current retrievals from actual spaceborne InSAR data was presented in [10], using data from the 11-day Shuttle Radar Topography Mission (SRTM) in early 2000: An SRTM-derived current field in the Wadden Sea off the Dutch coast was shown to agree quite well with a reference current field from a numerical circulation model; current variations on spatial scales of about 1 km were found to be resolved. In view

Manuscript received March 30, 2006; revised May 26, 2006. This work was supported by the University of Hamburg.

R. Romeiser is with the Institut für Meereskunde, Zentrum für Meeres- und Klimaforschung, Universität Hamburg, 20146 Hamburg, Germany (e-mail: romeiser@ifm.uni-hamburg.de).

H. Runge is with the Institut für die Methodik der Fernerkundung, Deutsches Zentrum für Luft-und Raumfahrt (DLR), 82234 Oberpfaffenhofen, Germany.

Digital Object Identifier 10.1109/TGRS.2006.885405

of the fact that the SRTM configuration was not optimized for current measurements, this was a quite positive finding. It was shown to be consistent with model results, indicating that the numerical InSAR imaging model M4S of the University of Hamburg [8], [11] permits realistic simulations of InSAR data products.

Operational (civilian) remote sensing satellites with ATI capabilities do not yet exist. However, the German satellite TerraSAR-X, which is scheduled for launch in late 2006, will carry an X-band SAR with a highly programmable phased array antenna panel. There are various possible modes of operation which would permit to configure different sections of the antenna array as individual receive antennas for moving target indication and velocity measurements by ATI. In this paper, we try to evaluate the suitability of these modes for ocean current measurements. The paper is structured as follows: In the following section, we review the relevant basic principles and requirements of ATI. In Section III, we give an overview of TerraSAR-X and its technical specifications and capabilities. Our procedure for simulating TerraSAR-X data products is described in Section IV, and results are presented and evaluated in Section V. Section VI deals with fundamental relations between along-track baseline, instrument noise, and resulting InSAR phase noise and possible ATI performance improvements that could be obtained, for example, by adding proposed passive extensions to the TerraSAR-X antenna panel. Finally, our main findings and conclusions are summarized in Section VII.

II. Along-Track InSAR Fundamentals

A conventional SAR exploits the Doppler history of backscattered signals for obtaining a high resolution in azimuth (flight) direction by synthesizing a long antenna aperture. This is done under the assumption that individual targets are not moving with respect to each other during the integration time, and the resulting SAR image does not provide a meaningful information on target velocities at individual pixels. However, two complex SAR images (each consisting of a real and imaginary part or an amplitude and phase for each pixel), acquired with a short time lag on the order of milliseconds and combined interferometrically, exhibit phase differences which are proportional to Doppler shifts of the backscattered signal and, thus, to line-of-sight velocities of the targets mapped into each individual pixel. As first proposed in [3] in 1987, this effect can be exploited for mapping ocean surface current fields. To obtain two SAR images with a short time lag from a moving platform, one needs two antennas separated by a corresponding distance in flight direction. Accordingly, the technique is called along-track interferometry (ATI). It should not be confused with (single-pass) cross-track interferometry, which uses two SAR antennas separated perpendicular to the flight direction, or repeat-pass interferometry, which uses two SAR images obtained during different overpasses of a test area on slightly different flight paths. The latter two techniques exploit phase differences resulting from different look angles from two antenna positions for deriving topographic maps [12], [13].

A crucial parameter of an along-track InSAR is the time lag τ between the two images, which is determined by the along-track distance L between the two antennas, the platform velocity V, and the mode of operation of the transmit/receive (T/R) chains: If both SAR antennas act as individual transmit and receive antennas, the phase centers of the relevant antenna patterns are separated by a baseline equal to the full distance L, and the corresponding InSAR time lag is $\tau = L/V$. If only one antenna is used for transmitting, the effective baseline reduces to $L/2$, thus $\tau = L/2V$. For current measurements, τ needs to be sufficiently long to obtain significant phase signatures of the current variations of interest and, at the same time, sufficiently short to avoid phase ambiguities (mapping of more than one realistic velocity interval into the phase interval of 2π) and a decorrelation of the backscattered signal, which would make interferometry impossible. According to theoretical analyses, ideal InSAR time lags for current measurements at X-band (about 10 GHz) are on the order of 2 to 5 ms [11]. On a spaceborne platform with a velocity on the order of 7000 m/s, this corresponds to effective along-track baselines of about 14 to 35 m.

Under ideal conditions, a spaceborne along-track InSAR would provide line-of-sight velocity maps at the high spatial resolution on the order of meters known from conventional SAR imagery. However, in the presence of considerable (zero-mean) thermal phase noise, some spatial averaging and a corresponding loss of resolution may be required for noise reduction. Furthermore, signatures of orbital wave motions resolved by the InSAR need to be filtered out if a true quasi-stationary surface current field without wave signatures is to be retrieved. Due to this latter problem, the effective spatial resolution of a single InSAR-derived current field will usually not be better than the wavelength of the dominant surface waves in the test area. Finally, one should be aware of the fact that an along-track InSAR is sensitive to surface currents only. This way, the technique is particularly attractive for applications in coastal waters, where surface currents do not differ very much from depth-averaged currents, and where subkilometer-scale spatial resolutions are appreciated. In contrast, radar altimetry, which is a well-established remote sensing technique for large-scale and mesoscale dynamic features in the upper layers of the open ocean, is not suitable for current retrievals in shallow waters and near coastlines. Accordingly, ATI and radar altimetry should be considered as complementary rather than competing techniques for current measurements.

An important limitation of the standard ATI concept lies in the fact that only line-of-sight velocity components are detected. In principle, this problem can be overcome by using two pairs of InSAR antennas whose beams are squinted at some angles forward and aft from broadside (dual-beam InSAR), as discussed first in [14], and as demonstrated recently with an experimental airborne system in [15]. The dual-beam InSAR permits fully two-dimensional velocity vector field measurements during a single overpass. Using a standard system with only two antennas, one can obtain two-dimensional current fields by combining data from at least two overpasses with different look directions, which is no major problem with an airborne system that permits several overpasses of the same test area within a few minutes. In contrast, the combined interpretation of satellite images from ascending and descending overpasses, which are

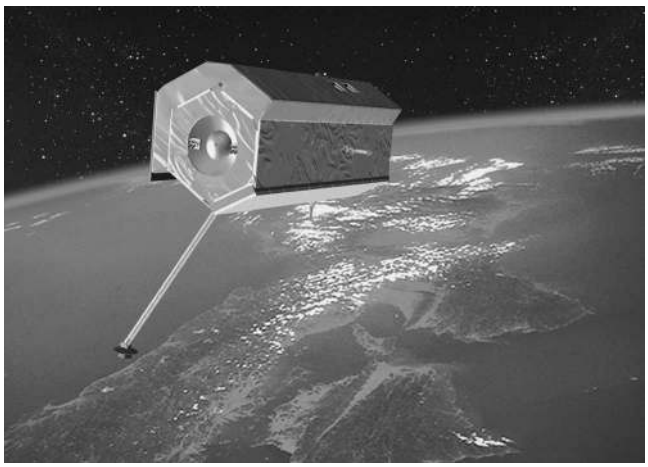

Fig. 1. Artist's view of TerraSAR-X in space. The SAR antenna is the light-gray panel facing downward; it is 4.8 m long. Copyright EADS Astrium.

usually separated by periods of several hours to days, is a much more challenging problem. However, some applications, such as shallow-water bathymetry retrievals or river runoff monitoring, do not depend on fully two-dimensional current measurements. In other cases, one can derive information on two-dimensional current properties by analyzing the data from a number of ascending and descending satellite overpasses statistically, or one can combine measured single-component current fields with hydrodynamic model computations to obtain two-dimensional vector current estimates.

III. TerraSAR-X

Fig. 1 shows an artist's view of the German satellite TerraSAR-X, which is scheduled for launch in early 2007. TerraSAR-X will carry an advanced high-resolution X-band (9.65 GHz) SAR system that can be operated in various modes. The mission will have a nominal lifetime of five years and is organized as a public–private partnership between the German Ministry of Education and Research, the German Aerospace Center, and EADS Astrium. TerraSAR-X will be in a sun-synchronous dawn-dusk orbit with a repeat cycle of 11 days at an altitude of 515 km and an inclination of 97.44° [16].

To form a variety of beam patterns for different swath widths, incidence angles, and spatial resolutions in different data-acquisition modes (Stripmap, ScanSAR, and Spotlight mode), TerraSAR-X will be equipped with a programmable phased array antenna consisting of 384 phase centers (12 columns in azimuth direction with 32 elements per column) with individual T/R modules that can be controlled independently [17]. Due to the possibility to use different sections of the array as individual antennas, this design will also permit ATI.

There are various possibilities to implement ATI modes with TerraSAR-X. A first concept of a divided antenna mode, also called split antenna mode or dual receive antenna (DRA) mode, was presented in 2002 in [18] and examined in further detail in [19] and [20]. It is based on the idea to split the antenna into two halves for receiving and feed their signals into two existing receive electronics chains. The ATI with an antenna separation of half the total antenna length of 4.8 m and an effective baseline of half the antenna separation, i.e., 1.2 m, would become possible this way. In addition, the classical DRA mode concept permits fully polarimetric measurements. However, the DRA mode uses the second receive chain of TerraSAR-X, which is mainly designed as a redundant component to guarantee the desired satellite life time. Furthermore, the acquisition and downlink of the conventional single-channel data will be impossible during DRA mode operations. Due to these facts, the availability of the DRA mode for oceanographic experiments will be quite limited.

Some of the technical limitations of the DRA mode can be overcome with another mode of operation proposed recently in [21]: In this mode, the antenna geometry and the effective along-track baseline remain the same as described above, but only a single receive electronics chain is used instead of two individual ones, being multiplexed between the two receiving antenna sections. This "aperture switching" requires a doubling of the pulse repetition frequency (PRF), but the high PRF is available anyway for the standard dual polarization mode of TerraSAR-X. Drawbacks [compared to the original DRA/dual receive chain (DRC) mode] are an increase of the instrument noise [noise equivalent sigma-zero (NESZ)] by 3 dB and a reduction of the swath widths (originally, 30 km for stripmap and 100 km for ScanSAR data acquisition) by a factor of 1/2. Furthermore, the increased PRF leads to increased azimuth ambiguities in the data processing, the compensation of which may require a reduction of the azimuth resolution and, possibly, a complete renouncement of ScanSAR data acquisitions [22].

The InSAR time lag obtained with two antenna halves of TerraSAR-X (effective along-track baseline $= 1.2$ m, platform velocity ≈ 7000 m/s) is about 0.17 ms, which is more than an order of magnitude shorter than optimal InSAR time lags at X-band [11] and a factor of 1/3 shorter than the time lag of the SRTM configuration used successfully for a first spaceborne ATI demonstration in [10]. To obtain longer time lags, one can think of further variations of the antenna section arrangement, such as concepts using only two 1/3 or 1/6 sections of the antenna array at the fore and aft ends. This way, improved effective baselines of 1.6 and 2.0 m, respectively, could be obtained, but the reduced effective antenna sizes would result in further increased noise levels and azimuth ambiguity problems.

IV. Simulation of InSAR Data Products of TerraSAR-X

To get an impression of the current measuring capabilities of TerraSAR-X in the different modes described above, we have simulated realistic data products with a numerical model and analyzed them statistically. The procedure resembles very much what was done in [10] with a simulated SRTM image of the Dutch Wadden Sea, which was shown to have very similar properties as the existing actual SRTM image of the test scenario. In this paper, we consider the same test scenario and use almost the same modeling procedure, current retrieval algorithm, and statistical analysis methods. This way, the results are comparable with those of the previous study and

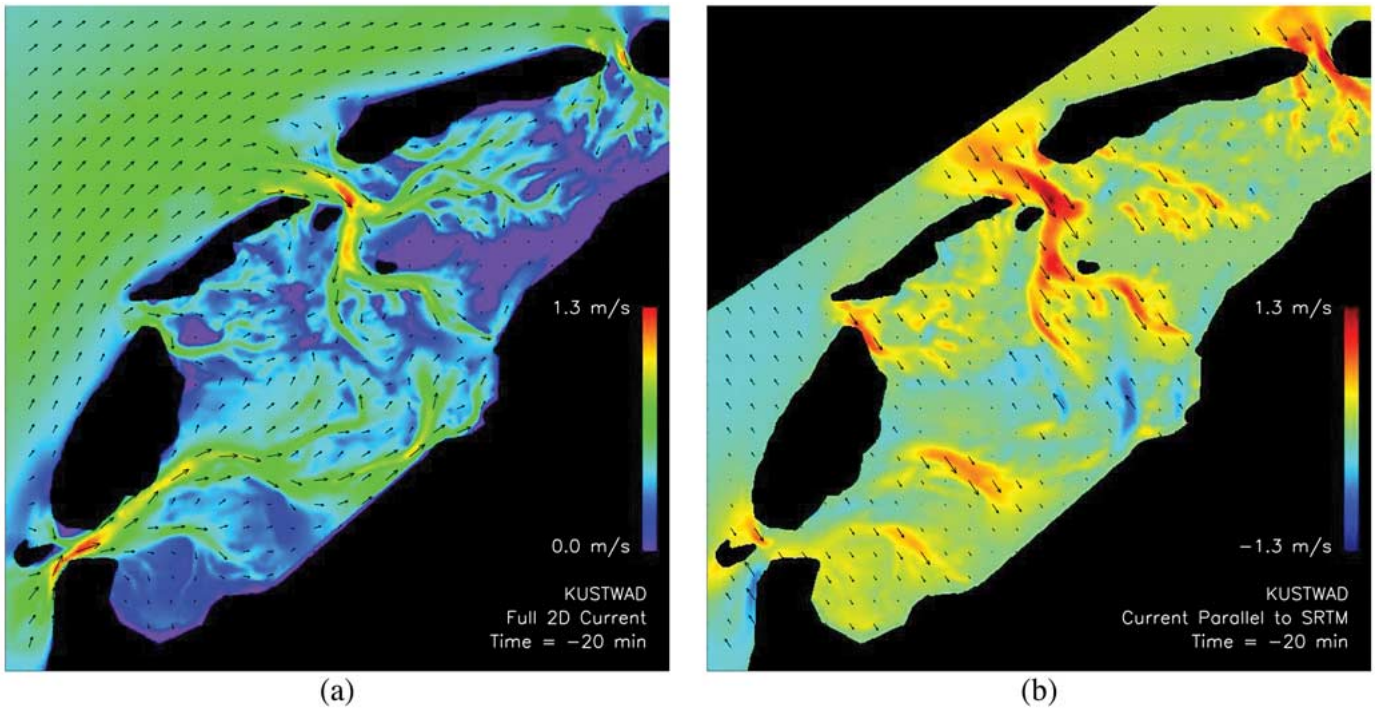

Fig. 2. Current field in the Dutch Wadden Sea as obtained from the circulation model KUSTWAD for the tidal phase 20 min before the overpass of SRTM in February 2000. (a) Full two-dimensional current field and (b) component parallel to the look direction of SRTM, only data points within the swath of SRTM. The shown area size is 70 km × 70 km. The shown grid resolution is 100 m × 100 m (after [10]).

enable us to relate the predicted current measuring performance of TerraSAR-X to the known performance of SRTM in the Wadden Sea case.

Fig. 2 shows a theoretical current field in the Dutch Wadden Sea which represents the conditions 20 min before the SRTM overpass on February 15, 2000. This current field, obtained from the Dutch numerical circulation model KUSTWAD [23], has already been used as a reference current field in [10]. Here, we use it again as an input current field for the InSAR simulations and as a reference for the statistical analyses. The total area of the current array, in which land, Lake IJssel, and the North Sea outside the swath of SRTM have been masked out, is 70 km × 70 km; the grid cell size is 100 m × 100 m. The wind speed during the SRTM overpass was about 5 m/s from west. To account for the wind dependence of InSAR signatures in the TerraSAR-X evaluations, simulations have been performed for wind speeds of 5, 10, and 15 m/s.

Simulated TerraSAR-X ATI images of the three test scenarios (one current field, three different wind speeds) have been obtained from the numerical model M4S of the University of Hamburg [11]. This model computes the Doppler spectra of the backscattered radar signal from each grid cell and converts them into expectation-value SAR and InSAR amplitude, phase, and coherence images, accounting for known artifacts of the SAR processing such as an azimuthal displacement of targets with a nonzero radial velocity and azimuthal blurring related to the Doppler bandwidth. Finally, realizations of intensity and phase images are obtained by applying a statistical model to the computed expectation-value arrays in combination with a given instrument noise level and number of independent looks per pixel or grid cell. Theoretically, the results have the same statistical properties and can be analyzed in the same way as actual satellite data.

In contrast to most previous studies with M4S, spatial variations of the surface wave spectrum due to hydrodynamic wave-current interaction and wind stress variations were not activated in the simulations for this paper. As shown in [11], such variations would normally cause nonlinearities in the InSAR imaging mechanism, which would become particularly strong at steep incidence angles. However, as discussed theoretically in [8] and [11] and demonstrated in [6], one can usually correct InSAR-retrieved velocity fields for this effect by an iterative correction scheme that modifies the input currents of a numerical InSAR imaging model until best possible agreement between the simulated and actually observed InSAR phase images (or Doppler velocity fields) is obtained. The optimized input current field resulting from this procedure is the best possible estimate of the true current field at the time of the InSAR data acquisition. Using exactly the same model for simulations of TerraSAR-X data products and the current retrieval procedure, we would obtain almost perfect corrections; thus, we can neglect the effects of spatially varying wave intensities from the beginning in the numerical simulations and analyses for this paper. Only the effects causing unrecoverable degradation of the data quality, such as phase noise and the blurring of images due to SAR processing, need to be taken into account for an evaluation of theoretically achievable current measuring accuracies and spatial resolutions. Nevertheless, one should keep in mind that the nonlinearities associated with spatially varying wave intensities increase strongly with a decreasing incidence angle. High (shallow) incidence angles will definitely facilitate the interpretation of along-track InSAR data and—given the

TABLE I
PARAMETERS OF THE CONSIDERED MODES OF TERRASAR-X

Mode of Operation[a]	Eff. Baseline	Inc. Angle	Looks per 10,000 m^2	NESZ[b] (DRC)	NESZ[b] (MPX)
2/2RA Stripmap[c]	1.2 m	20°	1036	–22.8 dB	–20.5 dB
		25°	1281	–21.7 dB	–19.3 dB
		30°	1515	–20.5 dB	–18.0 dB
		35°	1738	–19.2 dB	–16.6 dB
		40°	1948	–17.9 dB	–15.2 dB
2/2RA ScanSAR[d]	1.2 m	20°	178	–22.8 dB	–20.5 dB
		25°	220	–21.7 dB	–19.3 dB
		30°	260	–20.5 dB	–18.0 dB
		35°	299	–19.2 dB	–16.6 dB
		40°	335	–17.9 dB	–15.2 dB
2/3RA Stripmap[c]	1.6 m	20°	1036	–21.1 dB	–18.8 dB
		25°	1281	–20.0 dB	–17.6 dB
		30°	1515	–18.8 dB	–16.3 dB
		35°	1738	–17.5 dB	–14.9 dB
		40°	1948	–16.2 dB	–13.5 dB
2/3RA ScanSAR[d]	1.6 m	20°	178	–21.1 dB	–18.8 dB
		25°	220	–20.0 dB	–17.6 dB
		30°	260	–18.8 dB	–16.3 dB
		35°	299	–17.5 dB	–14.9 dB
		40°	335	–16.2 dB	–13.5 dB
2/6RA Stripmap[c]	2.0 m	20°	1036	–18.1 dB	–15.8 dB
		25°	1281	–17.0 dB	–14.6 dB
		30°	1515	–15.8 dB	–13.3 dB
		35°	1738	–14.5 dB	–11.9 dB
		40°	1948	–13.2 dB	–10.5 dB
2/6RA ScanSAR[d]	2.0 m	20°	178	–18.1 dB	–15.8 dB
		25°	220	–17.0 dB	–14.6 dB
		30°	260	–15.8 dB	–13.3 dB
		35°	299	–14.5 dB	–11.9 dB
		40°	335	–13.2 dB	–10.5 dB
SRTM[e]	3.5 m	55°	64	–29.0 dB	n/a

[a]) 2/2RA = 2/2 receive antennas, etc.; [b]) DRC = dual receive chain, MPX = multiplexed single receive chain; [c]) swath = 30 km / 15 km in DRC / MPX mode; [d]) swath = 100 km / 50 km in DRC / MPX mode; [e]) Shuttle Radar Topography Mission, swath width = 50 km

fact that the existing current retrieval and correction procedures are not perfect and not necessarily available to all potential users—lead to better real-world results in many cases.

For compatibility with the SRTM results, all TerraSAR-X simulations have been carried out for the data points covered by the SRTM swath and for the same look direction, while the actual coverage of the Wadden Sea test area by TerraSAR-X in its various modes of operation will—of course—differ from the SRTM coverage. To permit the use of a fixed model grid, the nominal single-look resolutions of all imaging modes were converted into corresponding effective numbers of independent looks per 100 m × 100 m grid cell. Along-track InSAR data obtained with two halves and with the outer two thirds and two sixths of the antenna panel have been considered with stripmap and ScanSAR resolutions, noise levels obtained with two independent receive chains (DRC) and a multiplexed single receive chain (MPX), incidence angles of 20°, 25°, 30°, 35°, and 40°, and vertical (VV) polarization. Key parameters of all considered modes of operation are given in detail in Table I, where information on spatial resolutions and noise level estimates has been obtained from [16]–[19] and [21] as well as from internal documents of the TerraSAR-X engineering team. Note that the instrument noise levels in our DRC and MPX simulations differ by less than the aforementioned nominal 3 dB. This mismatch results from the different swath widths of the DRC and MPX modes in combination with an increase of the instrument noise toward the boundaries of the full swaths in such a way that the effective mean noise levels across the respective swath widths differ by less than 3 dB. Note furthermore that Table I includes parameters of an SRTM simulation that was carried out for reference.

V. EVALUATION OF THE SIMULATION RESULTS

To get a first impression of the data quality, the simulated TerraSAR-X ATI phase images were processed by the same routines that had been applied to the actual and simulated SRTM data in [10]. The phase images with an original resolution of 100 m × 100 m were smoothed by applying a 5 × 5 pixel boxcar averaging filter three times (resulting in an effective resolution of about 500 m) and converted into horizontal line-of-sight velocities; mean biases with respect to the input/reference current field were subtracted. Two examples of simulated phase images and derived surface current fields are shown in Fig. 3. After this "standard" processing (with some additional highpass filtering to remove characteristic artifacts in the data), the SRTM image of the test area was shown to resolve current variations on spatial scales of about 1 km [10]. This data quality is our benchmark for the evaluation of the predicted TerraSAR-X results. In the following, we will relate various statistical properties of the simulated TerraSAR-X data products to the corresponding properties of the simulated SRTM data product and assume that the latter represents a typical InSAR-derived current field with an effective spatial resolution of about 1 km.

A. Overall Accuracy of the Retrieved Currents

Fig. 4 shows the overall rms differences between all simulated TerraSAR-X-derived current fields and the KUSTWAD current field. The reference value from the SRTM simulation is 0.058 m/s (gray horizontal line in diagrams). Most TerraSAR-X results (particularly the ones for stripmap data) are significantly below this value, which indicates a better signal-to-noise ratio (SNR) of the detected phases (averaged within the same spatial grid) with respect to SRTM case. Since TerraSAR-X has much higher instrument noise levels than SRTM (see Table I), the smallest rms errors are obtained at relatively steep incidence angles (20° to 30°) and higher wind speeds, where the normalized backscattering cross section (NRCS) of the ocean surface, thus the backscattered power and the SNR, becomes large. The observed increase of the rms error at steep incidence angles toward high wind speeds [Fig. 4(c) and (f)] can be attributed to an increased azimuthal blurring of SAR signatures due to the increased Doppler bandwidths, not to an increasing decorrelation of the backscattered signal (see Section VI).

Regarding the different modes of TerraSAR-X, the rms errors indicate that the quality of the ScanSAR data is clearly worse than the quality of the stripmap data, but the ScanSAR error levels at incidence angles of 20° to 30° and higher wind speeds are still better than the error level of the simulated SRTM result. Regarding the baseline selection, we find a small advantage of the "2/3RA" antenna arrangement with respect to the classical "2/2RA" arrangement that uses two full antenna halves for receiving. The "2/6RA" arrangement is the least favorable one;

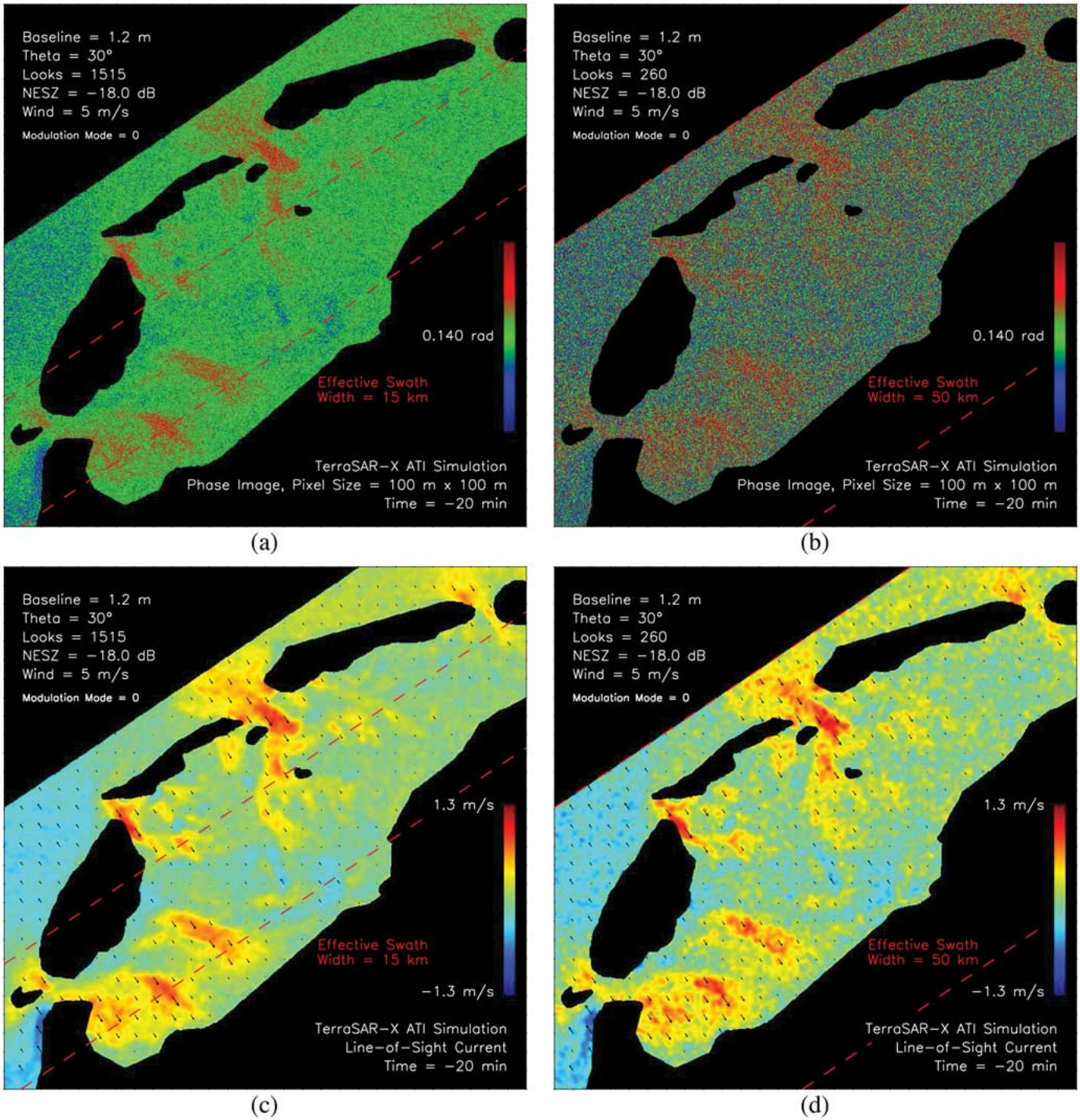

Fig. 3. Examples of the simulated TerraSAR-X along-track InSAR phase images (top) and line-of-sight current fields retrieved from these images by "standard" processing (bottom) for MPX stripmap (left) and ScanSAR (right) data acquisition, effective baseline $= 1.2$ m, incidence angle $= 30°$, and wind speed $= 5$ m/s.

particularly at higher incidence angles and ScanSAR resolution. Regarding the receive-chain setup (DRC or MPX; left/right column of Fig. 4), the rms error analysis does not indicate a major advantage of the DRC mode and its lower instrument noise levels. However, keep in mind that the swath width of MPX mode images is reduced by a factor of 1/2 with respect to the DRC mode, and that there may be problems with azimuth ambiguities and ScanSAR data processing in MPX mode (see Section III).

B. Spatial Resolution Analysis

So far, the overall rms errors indicate that several InSAR modes of TerraSAR-X will permit current measurements with a data quality superior to that of the SRTM-derived currents in the Dutch Wadden Sea. To characterize the data properties more quantitatively, we have carried out some analyses addressing achievable effective spatial resolutions.

Fig. 5 shows an example of how the rms error between the TerraSAR-X-derived current fields obtained from the two phase

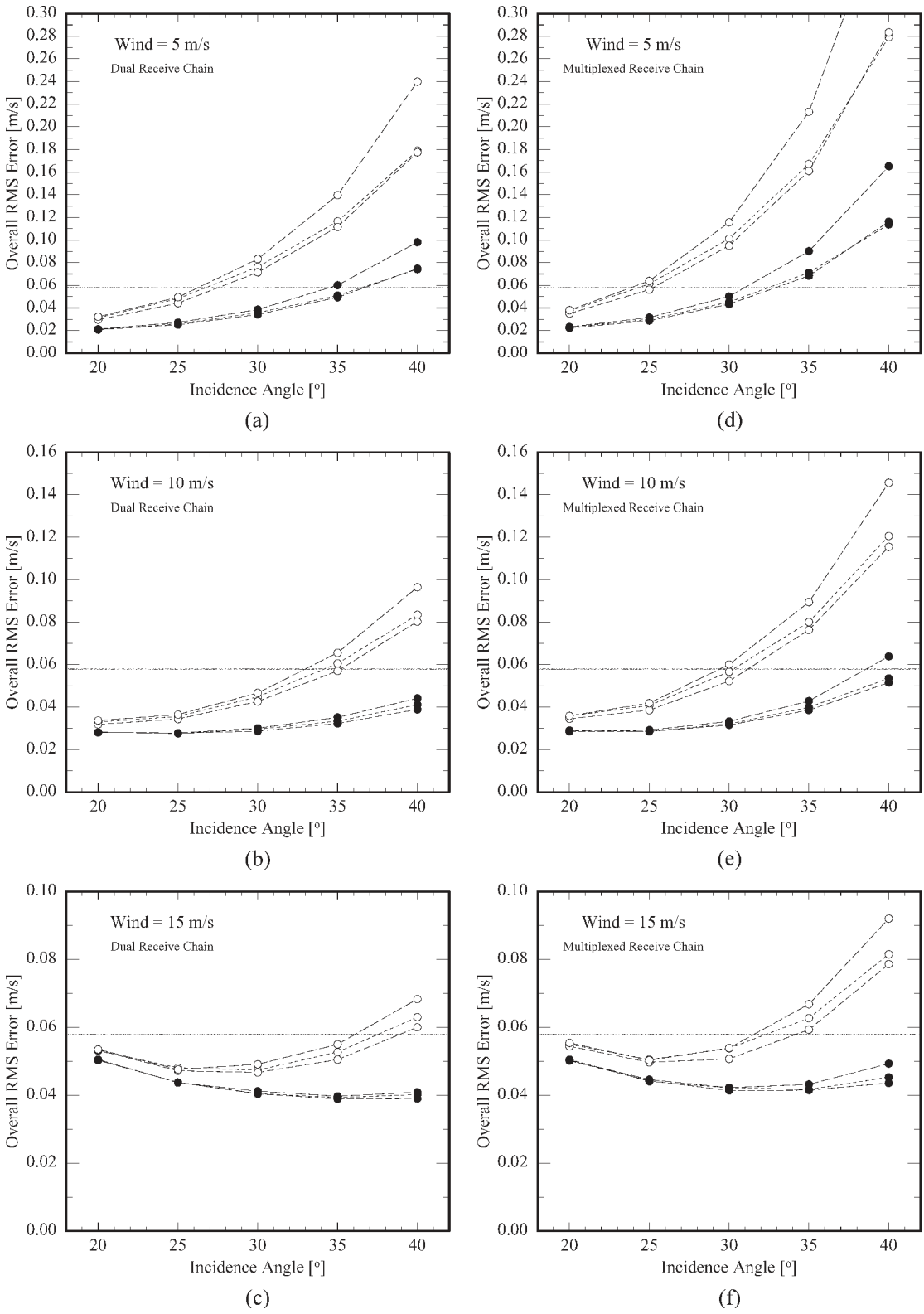

Fig. 4. Overall rms differences between the simulated TerraSAR-X-derived line-of-sight currents ("standard" processing) and reference currents versus incidence angle. Wind speed = 5 m/s (top), 10 m/s (center), and 15 m/s (bottom). DRC (left) and MPX (right) mode. Linestyle indicates effective baselines of 1.2 m (short-dashed), 1.6 m (longer dashed), and 2.0 m (long-dashed). Full circles = stripmap and open circles = ScanSAR. Gray horizontal line indicates rms error of simulated SRTM data product for comparison.

images of Fig. 3(a) and (b) and the reference current field depends on the spatial resolution. To obtain these diagrams, we have replaced the "standard" processing (three applications of a 5×5 pixel boxcar averaging filter before the conversion of InSAR phases into horizontal velocities) by the following procedure: The simulated phase images were directly converted into unsmoothed horizontal velocity arrays with independent pixel values at the original grid resolution of 100 m $\times$ 100 m.

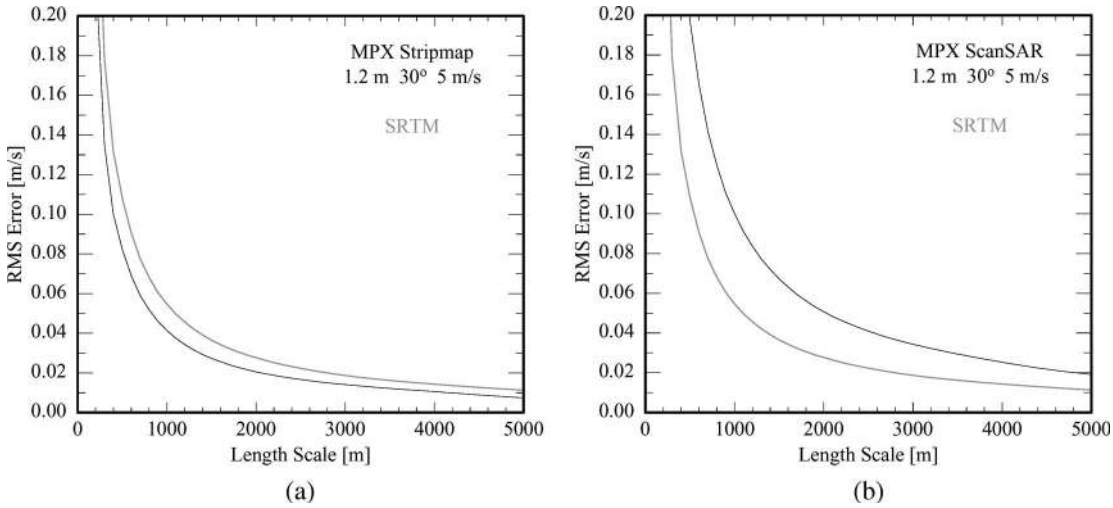

Fig. 5. Overall rms differences between the TerraSAR-X-derived currents corresponding to the two examples of Fig. 3 and reference currents, both smoothed with the same boxcar averaging filter, versus averaging length of the filter. (a) Stripmap data. (b) ScanSAR data. Gray line shows the result for simulated SRTM data product.

The resolutions of these arrays and of the reference current field (and, of course, the noise-induced fluctuations of the data) were then reduced by applying the boxcar averaging filters of increasing window size. The resulting overall rms errors as a function of window size are shown in the diagrams. The reference curve obtained for the SRTM simulation is shown as a gray line.

Consistent with Fig. 4(d), the diagrams of Fig. 5(a) and (b) show that the rms error of the currents derived from the stripmap image for MPX mode, a wind speed of 5 m/s, a baseline of 1.2 m, and an incidence angle of 30° is generally smaller than the rms error obtained for the SRTM simulation, while the rms error of the ScanSAR data product is larger. In other words, the stripmap data product reaches a given error level at a shorter averaging length (i.e., a higher effective spatial resolution) than the SRTM data product, while the ScanSAR data product requires more averaging (resulting in a lower effective spatial resolution) in this example.

Assuming that the SRTM-derived currents have an effective spatial resolution of 1000 m, we can define the effective resolution of a simulated data product of TerraSAR-X as the minimum averaging length at which the rms error becomes equal to the rms error of the simulated SRTM data product at an averaging length of 1000 m. Due to the different averaging procedures, this reference rms error is 0.055 m/s in this context, not the aforementioned 0.058 m/s of the "standard" product. Fig. 6 shows the results for all TerraSAR-X modes, incidence angles, and wind speeds. Based on the rms error criterion, the effective resolution of the TerraSAR-X stripmap data products will be better than 400 m, while the resolution of the ScanSAR data products will be better than 1000 m at higher wind speeds and worse at 5 m/s.

Of course, the relation between the rms error and effective resolution of an InSAR-derived current field depends on the strength of the spatial current variations to be detected: To obtain good estimates of current gradients at a given length scale, the relative error of each individual current estimate must be small compared to the current differences of interest. Fig. 7 shows the rms variabilities in the KUSTWAD current field and in the two example current fields from TerraSAR-X. Like in the previous analysis, the "length scale" is determined by the window size of a boxcar averaging filter. The computed rms variabilities are the rms differences between currents at grid points separated by the averaging length in range and azimuth (flight) direction, i.e., between the nearest grid points in the two directions that are statistically independent after averaging. The gray lines indicate that the variations in the KUSTWAD currents in the two directions increase monotonically with the considered length scale. The mean rms variability at a length scale of 1000 m is about 0.102 m/s, i.e., a little less than twice the rms error of the simulated SRTM data product at the same length scale. The variabilities of the two example TerraSAR-X data products [black lines in Fig. 7(a) and (b)] are quite high at short length scales, indicating high noise levels. They approach the variabilities in the KUSTWAD currents at length scales of a little less and a little more than 1000 m, respectively.

Fig. 8 shows the correlations between the spatial variations in the two example data products of TerraSAR-X (cf. Fig. 3) and the KUSTWAD currents as well as the corresponding results for the SRTM simulation. Again, we can look for the minimum averaging length at which the correlation for each individual simulated TerraSAR-X data product matches the correlation obtained for the SRTM simulation. Fig. 9 shows the results for all parameter combinations. They are very similar to the results obtained from the rms error analysis.

VI. Potential for Further Improvements

The good predicted current measuring capabilities of TerraSAR-X at quite short along-track InSAR baselines and corresponding short time lags may appear surprising in view of the fact that these time lags are about an order of magnitude shorter than the theoretical optimum of about 2 to 5 ms [11]. To validate that our findings are consistent with the previous theoretical results and recommendations and to get an impression

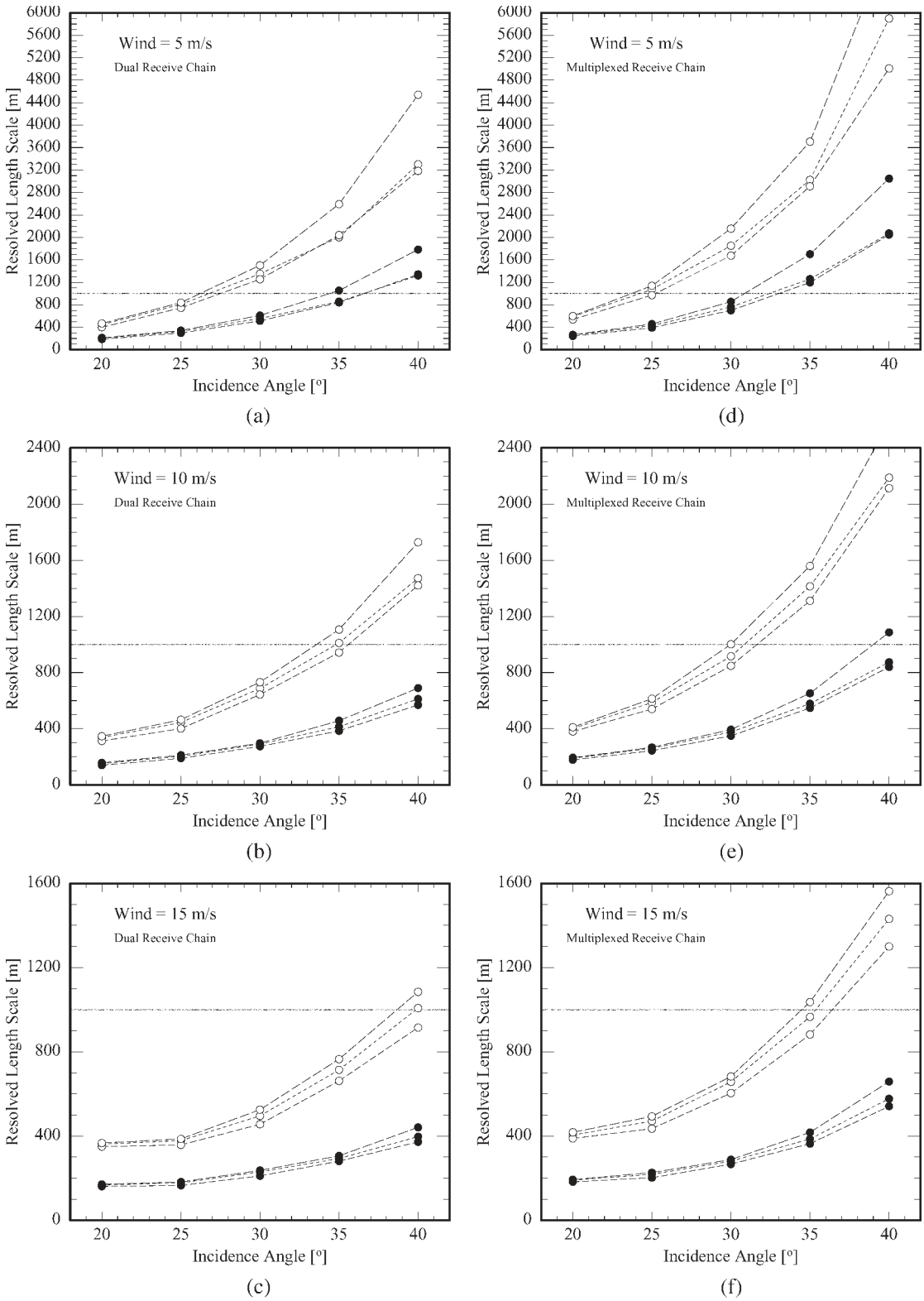

Fig. 6. Same as Fig. 4, but showing minimum averaging length scales at which the rms difference between the simulated TerraSAR-X-derived and reference currents becomes comparable to the rms difference between simulated SRTM-derived and reference currents after smoothing with an averaging length of 1000 m. Again, the linestyle indicates the effective baseline length (short-, longer, and long-dashed = 1.2, 1.6, and 2.0 m). Full circles = stripmap and open circles = ScanSAR. Gray line indicates corresponding SRTM result.

of possible further ATI performance improvements of TerraSAR-X type satellites, we can consider some fundamental relations. Fig. 10 shows (for three different wind speeds) how many independent interferogram samples need to be averaged at different baselines and noise levels to obtain horizontal velocity estimates with an accuracy of 0.1 m/s. The diagrams were derived from the results of statistical simulations based on theoretical NRCS values and Doppler bandwidths for

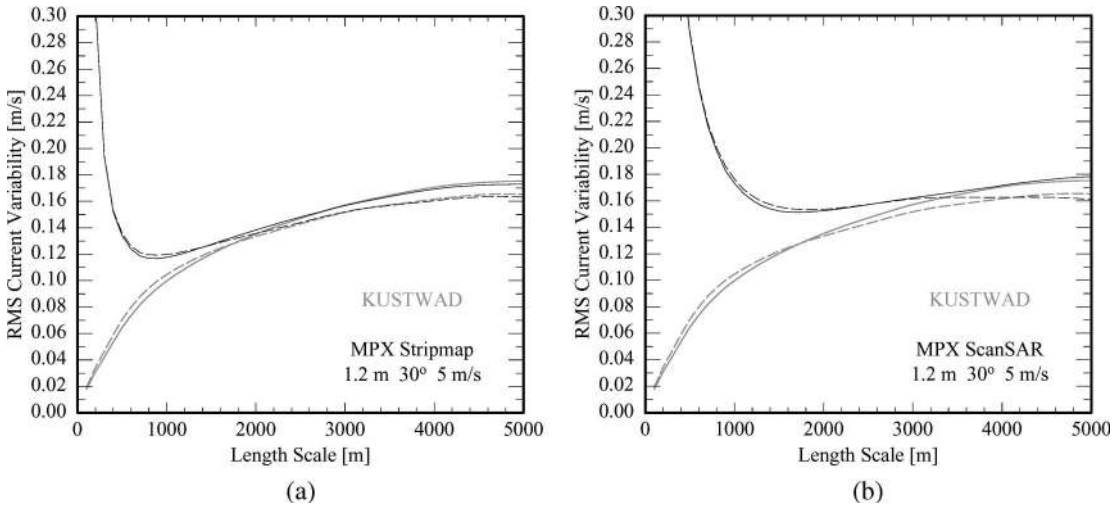

Fig. 7. RMS variabilities of smoothed TerraSAR-X-derived currents corresponding to the two examples of Fig. 3, i.e., rms differences between currents in adjacent grid points (separated by averaging length) versus averaging length. (a) Stripmap data. (b) ScanSAR data. Solid lines = variability in range direction, dashed lines = variability in azimuth direction. Gray lines show corresponding variabilities in the reference current field.

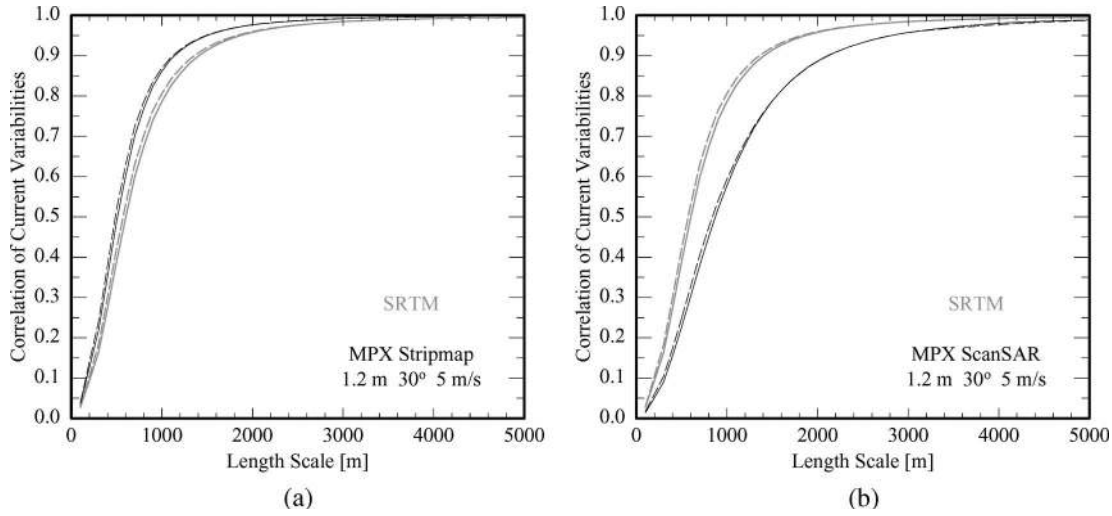

Fig. 8. Correlation between gradients of smoothed TerraSAR-X-derived currents corresponding to the two examples of Fig. 3 and corresponding gradients of smoothed reference currents versus averaging length. (a) Stripmap data. (b) ScanSAR data. Solid lines = gradients in range direction, dashed lines = gradients in azimuth direction. Gray lines show results for simulated SRTM data product.

X-band (9.65 GHz), VV polarization, and an incidence angle of 30° in combination with baselines between 1 and 100 m (and a platform velocity of 7000 m/s) and NESZ levels ranging from −30 to −9 dB in steps of 3 dB. Compared to our simulations for the Wadden Sea scenario, this is a more general analysis, but it does not account for any nonlinearities in the SAR/InSAR imaging mechanism of spatially varying current fields.

The diagrams depict that the required number of samples increases with the noise level and decreases with the baseline up to baseline lengths of about 10 to 50 m, depending on the wind speed and noise level. This decrease results from an increasing significance of the phase differences between the two backscattered signal vectors with respect to the baseline-independent instrument noise contributions. The following increase of the required number of samples toward longer baselines results from an increasing decorrelation of the backscattered signal during the increasing ATI time lag. Due to a faster temporal decay of the autocovariance of the backscattered signal at higher wind speeds, the required number of samples to be averaged at long baselines becomes larger with an increasing wind speed. In contrast, the required number of samples at short baselines decreases with an increasing wind speed, since temporal decorrelation is not a problem, while increasing the NRCS values leads to an improved SNR.

As a consistency check with our earlier results, we can revisit the statistical properties of the phase image of Fig. 3(a). According to the diagram of Fig. 5(a), velocity estimates with an rms error of 0.1 m/s are obtained from this image at an averaging window size of exactly 400 m × 400 m. Since the original phase image was obtained with 1515 independent looks in each pixel of 100 m × 100 m, this corresponds to a required number of samples of 24 240. This value is very close to the relevant corresponding value of the curve for −18 dB at a baseline of 1.2 m in Fig. 10(a). Accordingly, all of our findings are consistent. Moreover, the diagrams of Fig. 10 depict that there is a lot of potential for further accuracy improvements of

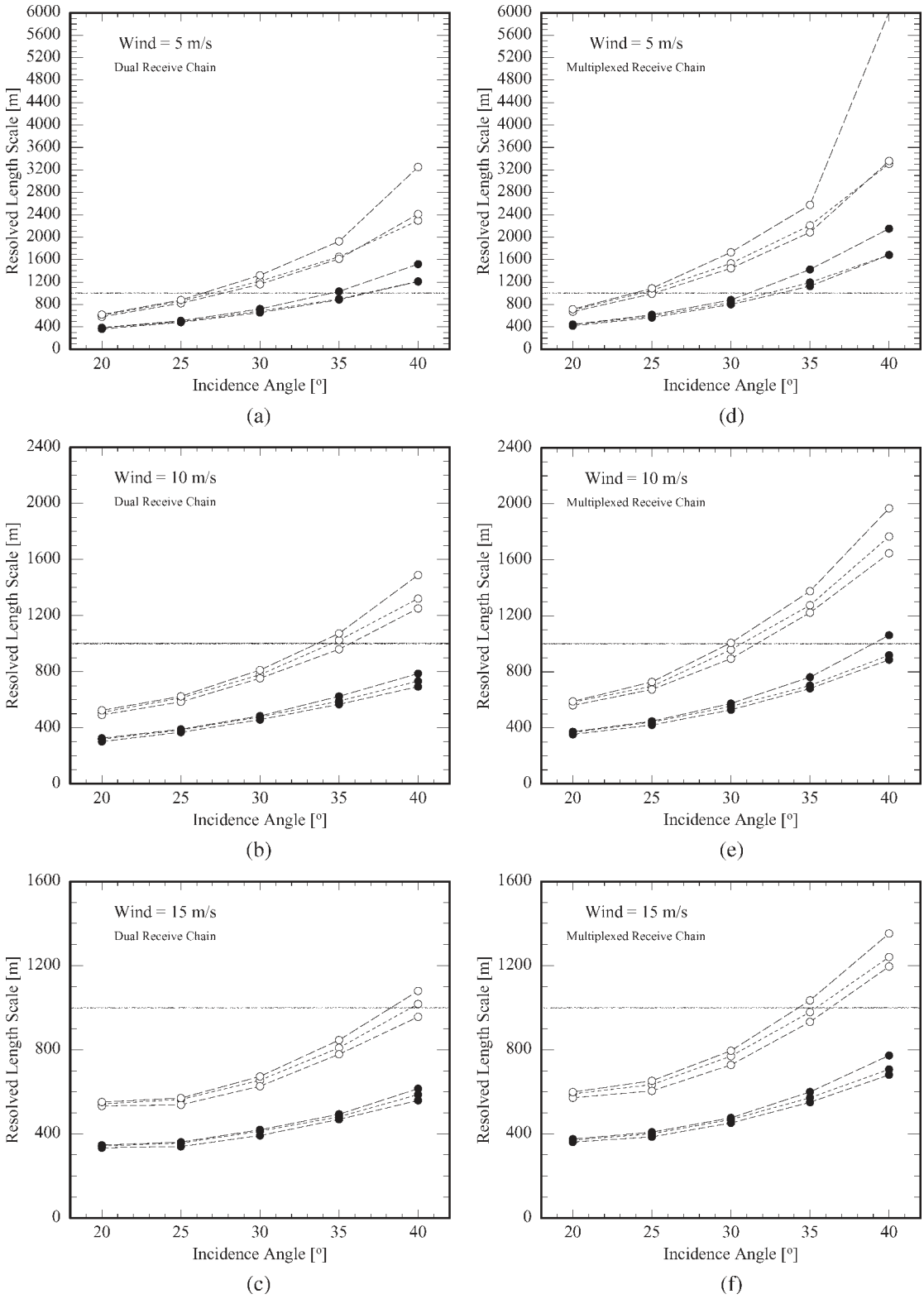

Fig. 9. Same as Fig. 6, but for mean correlation between current gradients in range and azimuth direction instead of rms difference between currents. Again, the linestyle indicates the effective baseline length (short-, longer, and long-dashed = 1.2, 1.6, and 2.0 m). Full circles = stripmap and open circles = ScanSAR. Gray line indicates corresponding SRTM result.

InSAR-derived currents at longer baselines or lower instrument noise levels. For example, a reduction of the instrument noise level of TerraSAR-X by a factor of 1/2 (-3 dB) would reduce the effective number of samples required to reach a given rms accuracy of the InSAR-derived currents by a factor of about 1/2. That is, the effective spatial resolution would be improved by a factor of $1/\sqrt{2}$ in both horizontal dimensions. Similarly, an increase of the effective baseline by a factor of two would even result in a reduction of the required number of samples by a factor of 1/4 (resolution improvement by a factor 1/2).

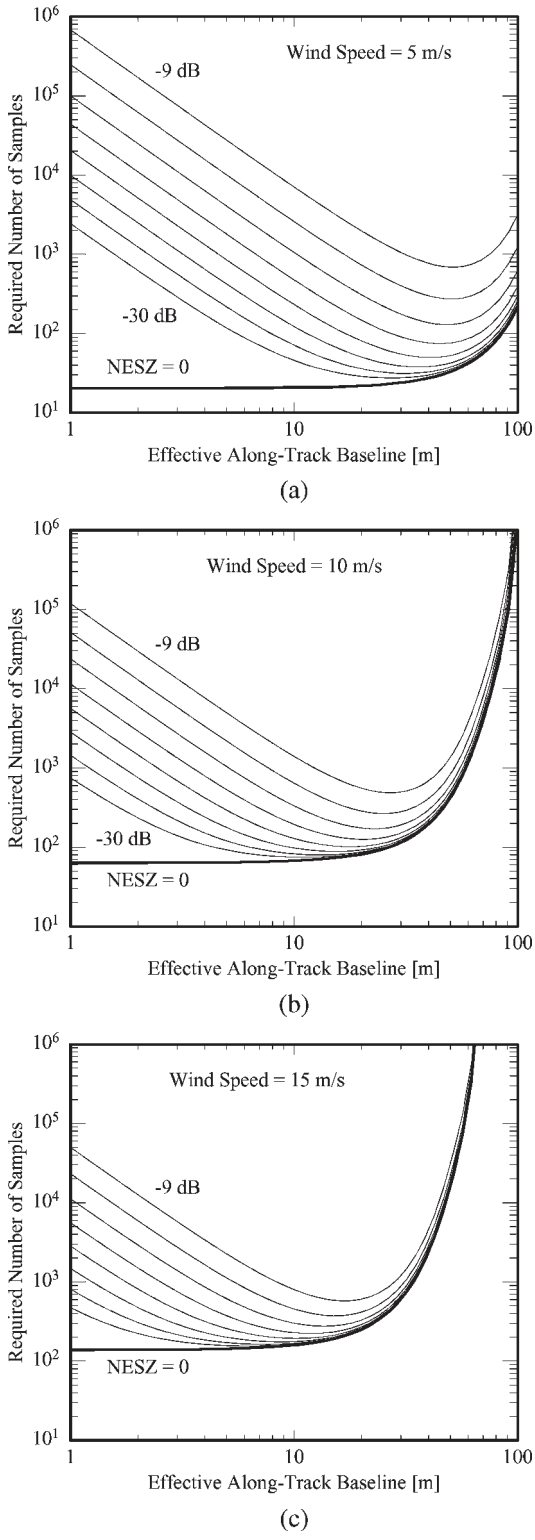

Fig. 10. Theoretical number of independent single-look interferogram samples to be averaged in order to obtain accurate velocity estimates (rms error of horizontal line-of-sight velocity $= 0.1$ m/s) versus effective along-track baseline, for instrument noise levels (NESZ) of 0 and -30 to -9 dB (in steps of 3 dB) and for wind speeds of (a) 5 m/s, (b) 10 m/s, and (c) 15 m/s. Other simulation parameters: Radar frequency $= 9.65$ GHz, polarization $=$ VV, incidence angle $= 30°$.

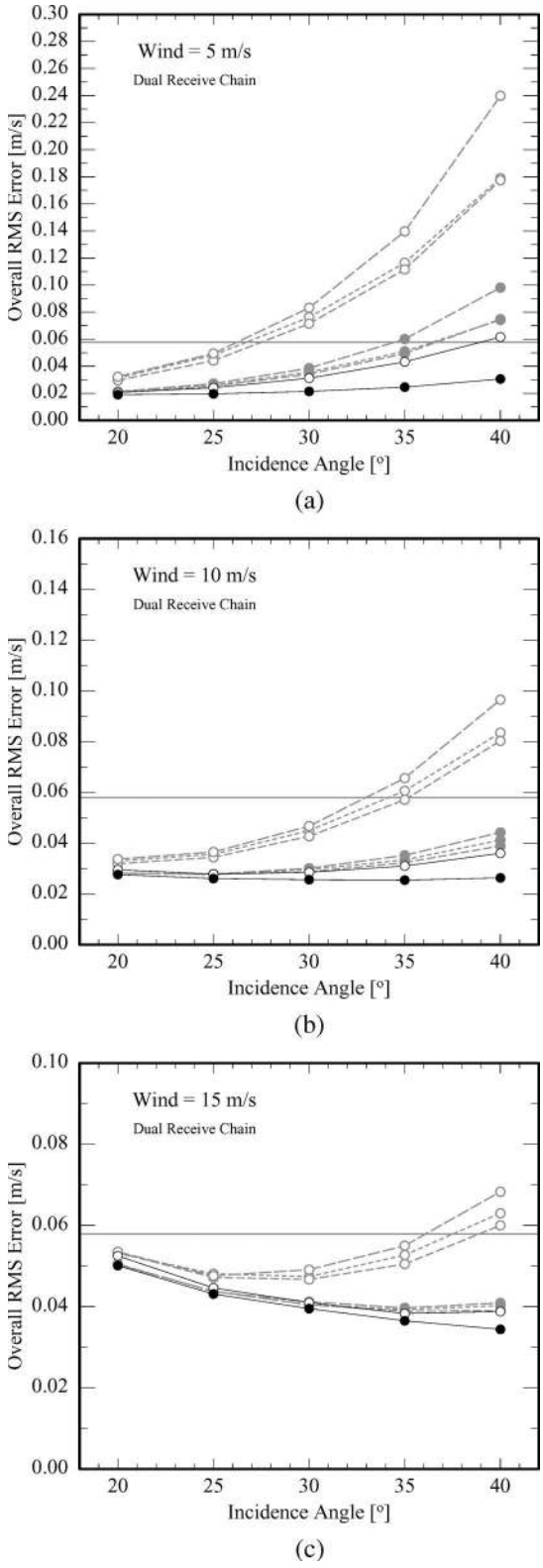

Fig. 11. Diagrams of Fig. 4 (now shown as gray dashed lines) with additional results for the proposed extended antenna array mode with an effective baseline of 3.6 m and DRC (black lines). Again, full circles and open circles indicate stripmap and ScanSAR operations, respectively, and the gray solid line indicates the relevant SRTM result.

In view of these findings, we would like to promote an idea for a possible upgrade of TerraSAR-X follow-on systems, which has already been presented in [21], and which could be realized with relatively simple hardware modifications: The upgrade consists of two passive (receive-only) antenna extensions of 2.4 m each at the fore and aft ends of the unaltered main

antenna panel. Using the full main antenna panel for transmitting (as in all other examples) and only the two outside panels with individual receive chains for receiving, one would obtain an effective baseline of 3.6 m in combination with the noise level and swath widths of the original DRA/DRC mode. Diagrams characterizing the data quality obtained from this configuration are shown in Figs. 11–13. The effective spatial resolutions at an incidence angle of 30° are found to be on the order of 100 to 300 m for stripmap and 300 to 600 m for ScanSAR data, which is much better than the resolution of SRTM in the Wadden Sea case and also a major improvement with respect to the other considered InSAR modes of TerraSAR-X. Good spatial resolutions would be obtained even at an incidence angle of 40°, which may be more attractive than 30° for some applications in view of the reduced nonlinearities of the imaging mechanism. Another advantage of an InSAR configuration like this with several independent antenna sections and receive chains would be the possibility to perform multibaseline ATI as described in [24], permitting full Doppler spectrum estimates in each pixel and corresponding improvements of the effective spatial resolution of the images and the retrievable geophysical information content.

VII. Conclusion

We have presented a comprehensive analysis of current measuring capabilities of the upcoming German satellite TerraSAR-X in various possible along-track InSAR modes. Depending on the antenna and receiver settings, effective along-track baselines of 1.2, 1.6, and 2.0 m can be obtained in combination with the different swath widths (15, 30, 50, and 100 km), nominal spatial resolutions, and instrument noise levels. The current measuring performance in these different modes has been evaluated at different incidence angles (20° to 40°) and wind speeds (5 to 15 m/s) on the basis of numerical simulations and different techniques for determining the effective accuracy and spatial resolution of the simulated InSAR-derived current fields.

Our results indicate that all considered along-track InSAR modes of TerraSAR-X will permit current measurements with a data quality comparable or superior to the data quality obtained from an SRTM image of the Dutch Wadden Sea in February 2000. While the SRTM data product was shown to have an effective spatial resolution of about 1 km in an earlier study [10], we have found effective resolutions on the order of 400 to 800 m (stripmap data) or 600 to 1500 m (ScanSAR data) for TerraSAR-X, where the swath widths are 15 or 30 km for stripmap and 50 or 100 km for ScanSAR data, depending on the receive-chain arrangement (MPX and DRC, respectively). Aside from the reduced swath width and increased azimuth ambiguities, which may have particularly negative effects on ScanSAR data, the newly proposed MPX mode, which may be available more frequently than the classical DRA/DRC mode, will deliver almost the same data quality. The most favorable antenna setting for interferometric current measurements uses the full antenna panel for transmitting and the fore and aft 1/3 for receiving with an effective along-track baseline of 1.6 m, but the improvement with respect to the classical arrangement with two full antenna halves and a baseline of 1.2 m is small. For a good tradeoff between an increasing SNR

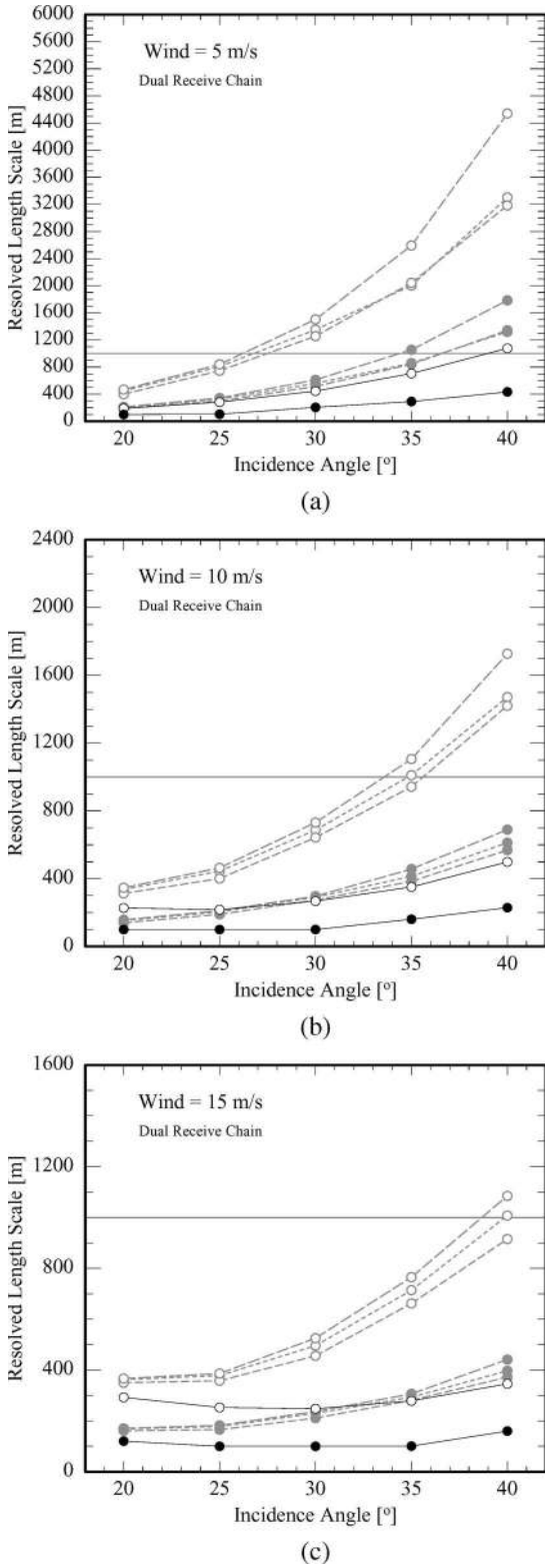

Fig. 12. Diagrams of Fig. 6 (now shown as gray dashed lines) with additional results for the proposed extended antenna array mode with an effective baseline of 3.6 m and DRC (black lines). Again, full circles and open circles indicate stripmap and ScanSAR operations, respectively, and the gray solid line indicates the relevant SRTM result.

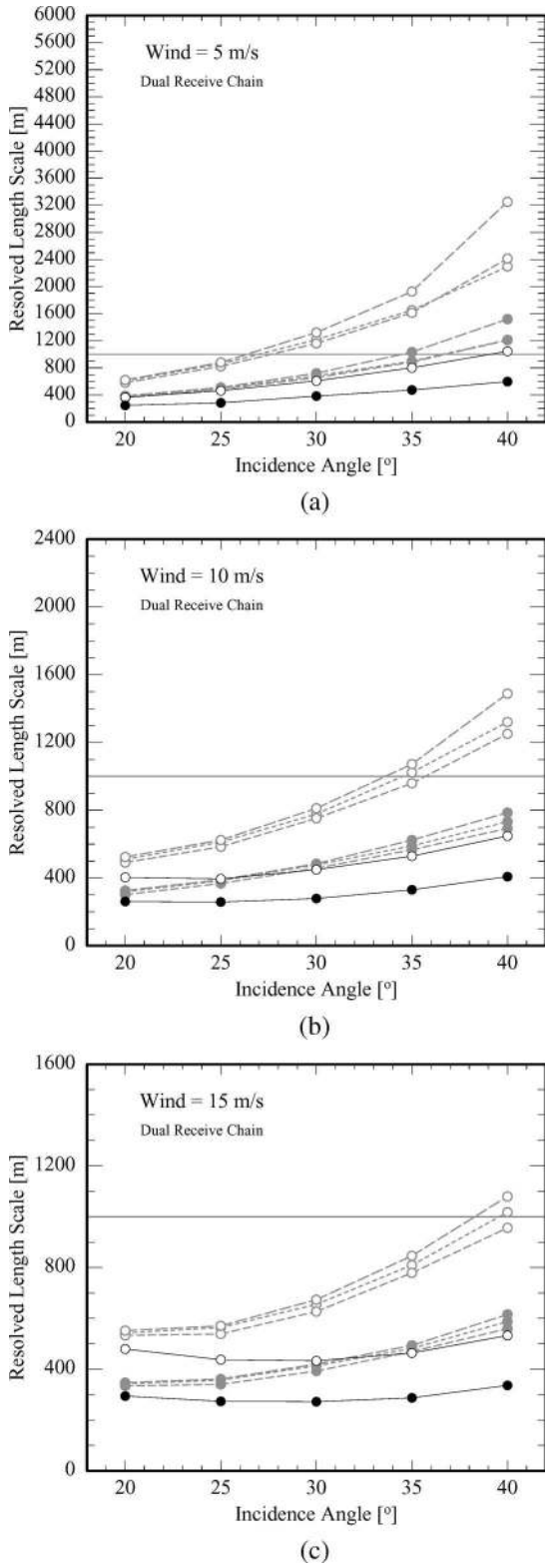

Fig. 13. Diagrams of Fig. 9 (now shown as gray dashed lines) with additional results for the proposed extended antenna array mode with an effective baseline of 3.6 m and DRC (black lines). Again, full circles and open circles indicate stripmap and ScanSAR operations, respectively, and the gray solid line indicates the relevant SRTM result.

and increasing nonlinearities of the ATI imaging mechanism toward steep incidence angles, we recommend incidence angles around 30°.

In view of the fact that TerraSAR-X has not been designed for current measurements originally, the predicted performance is quite good. If our performance predictions are correct, the use of TerraSAR-X for current measurements will be limited mainly by the availability of the experimental modes of operation and by the limited spatial coverage resulting from narrow swath widths, but not by the data quality. To demonstrate the ATI capabilities of TerraSAR-X at the best possible data quality and spatial coverage, it is highly desirable to obtain at least a few images of selected test areas in the classical DRA/DRC mode with stripmap and ScanSAR data acquisition. Given the fact that a demand for repeated high-resolution current measurements has been formulated quite clearly by the potential user community, we believe that a successful demonstration of repeated current measurements from space may attract the interest of many potential users and lead to an implementation of operationalized and further improved along-track InSAR concepts on TerraSAR-X follow-on satellites. A first possible upgrade has been discussed in Section VI of this paper; it consists of an extended antenna panel with an effective along-track baseline of 3.6 m and a fully operational DRC. With this upgrade, spatial resolutions on the order of 500 m can be obtained even for ScanSAR data with a swath width of 100 km, and possible full Doppler spectrum estimates on the basis of multibaseline InSAR data may result in further improved capabilities. On the long term, the developments may even lead to an implementation of spaceborne dual-beam along-track InSARs for fully two-dimensional current measurements; using the technique that has already been demonstrated by American scientists with an airborne prototype system.

ACKNOWLEDGMENT

The authors would like to thank K. de Jong and J. Vogelzang from Rijkswaterstaat, Netherlands, for providing the KUSTWAD data and the TerraSAR-X engineering team for numerous fruitful discussions.

REFERENCES

[1] J. Fischer and N. C. Flemming, *Operational Oceanography: Data Requirements Survey*. Southampton, U.K.: Southampton Oceanography Centre, 1999. EuroGOOS Publication No. 12.

[2] H. H. Essen, K. W. Gurgel, and T. Schlick, "On the accuracy of current measurements by means of HF radar," *IEEE J. Ocean. Eng.*, vol. 25, no. 4, pp. 472–480, Oct. 2000.

[3] R. M. Goldstein and H. A. Zebker, "Interferometric radar measurement of ocean surface currents," *Nature*, vol. 328, no. 6132, pp. 707–709, Aug. 1987.

[4] D. R. Thompson and J. R. Jensen, "Synthetic aperture radar interferometry applied to ship-generated waves in the 1989 Loch Linnhe experiment," *J. Geophys. Res.*, vol. 98, no. C6, pp. 10 259–10 269, 1993.

[5] H. C. Graber, D. R. Thompson, and R. E. Carande, "Ocean surface features and currents measured with synthetic aperture radar interferometry and HF radar," *J. Geophys. Res.*, vol. 101, no. C11, pp. 25 813–25 832, 1996.

[6] R. Romeiser, "Current measurements by airborne along-track InSAR: Measuring technique and experimental results," *IEEE J. Ocean. Eng.*, vol. 30, no. 3, pp. 552–569, Jul. 2005.

[7] D. Massonnet, E. Thouvenot, S. Ramongassié, and L. Phalippou, "A wheel of passive radar microsats for upgrading existing SAR projects," in *Proc. IGARSS*, Honolulu, HI, 2000, pp. 1000–1003.

[8] R. Romeiser, M. Schwäbisch, J. Schulz-Stellenfleth, D. R. Thompson, R. Siegmund, A. Niedermeier, W. Alpers, and S. Lehner, "Study on

concepts for radar interferometry from satellites for ocean (and Land) applications (KoRIOLiS)," Univ. Hamburg, Hamburg, Germany, Final Report 50EE0100, 2002. 112 p. [Online]. Available: http://www.ifm.uni-hamburg.de/~romeiser/koriolis.htm

[9] A. Moreira, G. Krieger, I. Hajnsek, D. Hounam, M. Werner, S. Riegger, and E. Settelmeyer, "TanDEM-X: A TerraSAR-X add-on satellite for single-pass SAR interferometry," in *Proc. IGARSS*, Anchorage, AK, 2004, pp. 1000–1003.

[10] R. Romeiser, H. Breit, M. Eineder, H. Runge, P. Flament, K. de Jong, and J. Vogelzang, "Current measurements by SAR along-track interferometry from a space shuttle," *IEEE Trans. Geosci. Remote Sens.*, vol. 43, no. 10, pp. 2315–2324, Oct. 2005.

[11] R. Romeiser and D. R. Thompson, "Numerical study on the along-track interferometric radar imaging mechanism of oceanic surface currents," *IEEE Trans. Geosci. Remote Sens.*, vol. 38, no. 1, pt. 2, pp. 446–458, Jan. 2000.

[12] L. C. Graham, "Synthetic interferometer radar for topographic mapping," *Proc. IEEE*, vol. 62, no. 6, pp. 763–768, Jun. 1974.

[13] H. Zebker and R. Goldstein, "Topographic mapping from interferometric SAR observations," *J. Geophys. Res.*, vol. 91, no. B5, pp. 4993–4999, 1986.

[14] S. J. Frasier and A. J. Camps, "Dual-beam interferometry for ocean surface current vector mapping," *IEEE Trans. Geosci. Remote Sens.*, vol. 39, no. 2, pp. 401–414, Feb. 2001.

[15] J. V. Toporkov, D. Perkovic, G. Farquharson, M. A. Sletten, and S. J. Frasier, "Sea surface velocity vector retrieval using dual-beam interferometry: First demonstration," *IEEE Trans. Geosci. Remote Sens.*, vol. 43, no. 11, pp. 2494–2502, Nov. 2005.

[16] A. Roth, *TerraSAR-X Science Plan*. Munich, Germany: DLR Oberpfaffenhofen, 2004. [Online]. Available: http://www.caf.dlr.de/tsx/documentation/TSX-Science-Plan.pdf

[17] M. Suess, S. Riegger, W. Pitz, and R. Werninghaus, "TerraSAR-X—Design and performance," in *Proc. EUSAR*, Cologne, Germany, Jun. 4–6, 2002, pp. 49–52.

[18] J. Mittermayer, V. Alberga, S. Buckreuss, and S. Riegger, "TerraSAR-X: Predicted performance," in *Proc. SPIE 9th Int. Symp. Remote Sens.*, Crete, Greece, 2002. 12 p.

[19] J. Mittermayer and H. Runge, "Conceptual studies for exploiting the TerraSAR-X dual receive antenna," in *Proc. IGARSS*, Toulouse, France, 2003, pp. 2140–2142.

[20] R. Romeiser, H. Breit, M. Eineder, H. Runge, P. Flament, K. de Jong, and J. Vogelzang, "On the suitability of TerraSAR-X split antenna mode for current measurements by along-track interferometry," in *Proc. IGARSS*, Toulouse, France, 2003, pp. 1320–1322.

[21] H. Runge, M. Eineder, G. Palubinskas, S. Suchandt, and F. Meyer, "Traffic monitoring with TerraSAR-X," in *Proc. IRS*, Berlin, Germany, 2005, pp. 629–634.

[22] H. Runge *et al.*, "Performance analysis of virtual multi-channel modes for TerraSAR-X," in *Proc. EUSAR*, 2006.

[23] H. H. ten Cate, S. Hummel, and M. R. T. Roest, "An open model system for 2d/3d hydrodynamic simulations," in *Proc. Hydroinformatics*, Iowa City, IA, 2000.

[24] B. Friedlander and B. Porat, "VSAR: A high resolution radar system for ocean imaging," *IEEE Trans. Aerosp. Electron. Syst.*, vol. 34, no. 3, pp. 755–776, Jul. 1998.

Roland Romeiser (M'00) received the Dipl.-Phys. degree in physics from the University of Bremen, Bremen, Germany, in 1990, and the Dr.rer.nat. degree from the University of Hamburg, Hamburg, Germany, in 1993.

He is currently a Permanent Staff Scientist with the Institute of Oceanography of the University of Hamburg. He has wide experience in the remote sensing of ocean currents, waves, and winds by various microwave sensors. He has been involved in a number of national and international remote sensing projects and experiments. His current research focuses on the theoretical modeling of SAR and InSAR signatures of spatially varying ocean surface currents and the development and evaluation of current retrieval techniques.

Dr. Romeiser has organized and chaired several sessions at international remote sensing conferences. From August 1998 to July 1999, he spent a year with the Johns Hopkins University/Applied Physics Laboratory, Laurel, MD, as a Feodor Lynen Fellow of the Alexander von Humboldt Foundation. Since fall 2000, he has been an Associate Editor of the IEEE JOURNAL OF OCEANIC ENGINEERING.

Hartmut Runge received the Dipl.-Ing. degree in electrical engineering/communications from the University of Siegen, Siegen, Germany in 1980.

Since 1980, he has been a DLR Staff Member and working on various aspects of SAR data processing and applications. He was the Systems Engineer with the Processing and Archiving Facility (PAF) for the X-SAR missions in 1996 and the Project Manager with the X-SAR data processing subsystem for the Shuttle Radar Topography Mission (SRTM) in 2000. Furthermore, he was the Principal Investigator with the SRTM along-track interferometry (ATI) experiments and pioneered the measurement of moving objects like cars and ocean currents from a spaceborne sensor. He worked on concepts for a close satellite formation flight for ATI. For six months, he worked with the Toulouse Space Centre of CNES for the cartwheel project and formed a joint DLR/CNES research team. He initiated the implementation of an ATI mode on the TerraSAR-X satellite and is currently the Project Manager with the "TerraSAR-X Traffic Monitoring Project."